ACS APPLIED MATERIALS & INTERFACES

www.acsami.org

Research Article

Near-Infrared Photothermal/Photodynamic-in-One Agents Integrated with a Guanidinium-Based Covalent Organic Framework for Intelligent Targeted Imaging-Guided Precision Chemo/PTT/PDT Sterilization

Yu-Shi Liu, Xiang Wei, Xu Zhao,* Li-Jian Chen, and Xiu-Ping Yan*

Cite This: *ACS Appl. Mater. Interfaces* 2021, 13, 27895−27903

Read Online

ACCESS | Metrics & More | Article Recommendations | Supporting Information

ABSTRACT: Phototherapy holds great promise in the treatment of bacterial infections, especially the multidrug resistant bacterial infections. However, most therapeutic agents are based on the integration of individual photothermal agents and photosensitizers, always in the activated state, and generally lack bacterial specificity, resulting in uncertain pharmacokinetics and serious nonspecific damage to normal tissues. Herein, we report a pH-responsive nanoplatform with synergistic chemo-phototherapy function for smart fluorescence imaging-guided precision sterilization. pH reversible activated symmetric cyanine was designed and prepared as a bacterial-specific imaging unit and PTT/PDT-in-one agent. Meanwhile, a guanidinium-based covalent organic framework (COF) was employed as a nanocarrier and chemotherapy agent to build the intelligent nanoplatform via electrostatic self-assembly. The self-assembly of the PTT/PDT-in-one agent and the COF greatly improves the stability and blood circulation of the PTT/PDT-in-one agent and provides charge-reversed intelligent targeting ability. The developed smart nanoplatform not only enables bacterial-targeted imaging but also possesses chemo/PTT/PDT synergetic high-efficiency bactericidal effects with little side effects, showing great potential in practical applications.

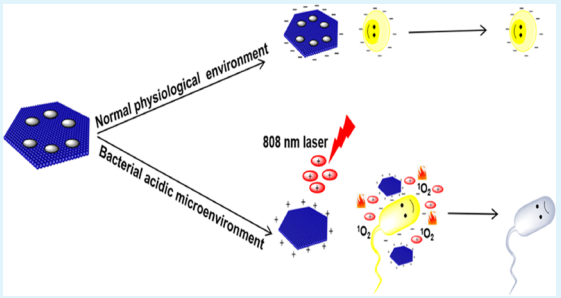

KEYWORDS: *pH reversible activation, photothermal/photodynamic-in-one probe, NIR fluorescence imaging, charge reversal-targeting, precision sterilization*

INTRODUCTION

Bacterial infections seriously threaten human health and social development. Antibiotics are the most accepted treatment and have been widely used for bacterial infections. However, the overuse of antibiotics has led to the emergence of a large number of drug-resistant bacteria, weakening the therapeutic effect, leading to high mortality and seriously wasted medical resources.[1−4] Therefore, it is imperative to develop revolutionary treatment strategies for bacterial infections.

Phototherapy, a promising therapeutic modality with the advantages of noninvasiveness, nondrug resistance, and low toxicity, shows great potential to revolutionize traditional antimicrobial methods.[5,6] Phototherapy including photothermal (PTT) and photodynamic (PDT) therapy is a method of inducing bacterial damage by generating heat or reactive oxygen species in the presence of therapeutic agents, an appropriate light source, and oxygen.[7−9] However, therapeutic agents, the most core factor of phototherapy, are mostly based on the integration of individual PTT and PDT agents[10−12] and even require two-wavelength excitation light irradiation,[13−15] resulting in asynchronous treatment, superimposed side effect, and prolonged treatment time. In addition, most of the conventional therapeutic agents lack bacterial targeting and are often in the "always on" activated state, causing nonspecific damage to normal tissues.[16,17] Therefore, it is of great importance to develop single-wavelength activated PTT/PDT integrated intelligent therapeutic agents.

Targeting strategies can enhance the bacterial uptake of therapeutic agents and provide therapeutic efficiency to a certain extent. Traditional targeting strategies are mostly based on the functionalization of bacterial-specific ligands[18,19] or cations.[20,21] The lack of universality and safety of ligands greatly impair active targeting efficiency.[22] Moreover, cation-functionalized therapeutic agents are easily recognized and metabolized by phagocytes, resulting in too low drug concentration at the site of infection to achieve the desired therapeutic effect.[23,24] Anaerobic fermentation caused by

Received: March 28, 2021
Accepted: May 26, 2021
Published: June 8, 2021

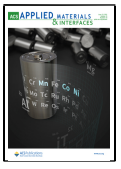

https://doi.org/10.1021/acsami.1c05705
ACS Appl. Mater. Interfaces 2021, 13, 27895−27903

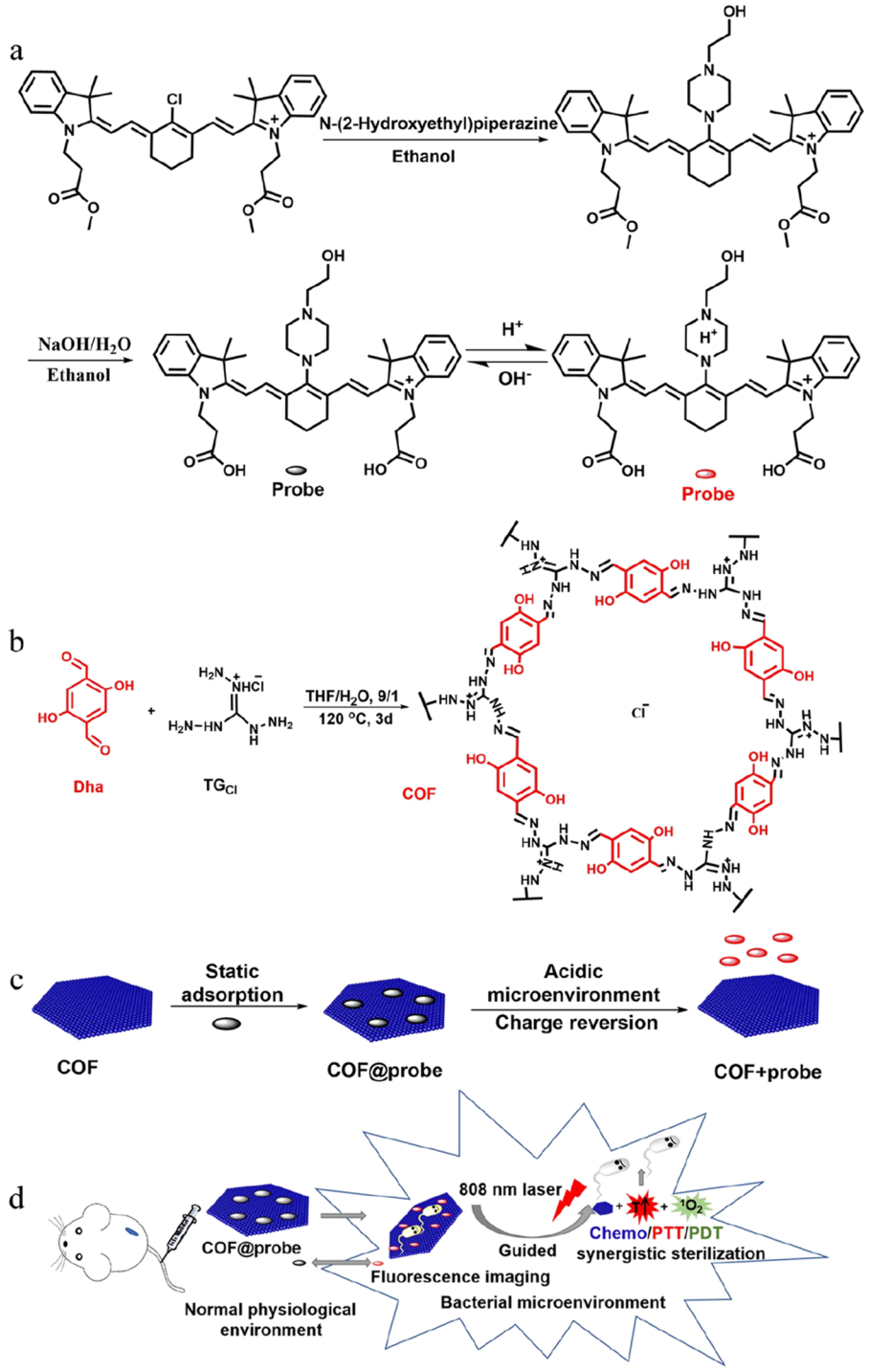

Figure 1. Design strategy and schematic of the COF@probe theranostic platform: (a) Synthetic route of the PTT/PDT-in-one agent. (b) Synthetic route of the COF. (c) Schematic diagram for the preparation of the COF@probe platform. (d) Illustration of the COF@probe theranostic platform for precision imaging-guided chemo/PTT/PDT synergistic sterilization.

hypoxia and inflammation at the bacterial infected site often results in a local decrease in pH.[25−28] The acidic microenvironment feature enables the development of intelligent targeted and responsive therapeutic platforms to meet the requirements of bacterial-targeted aggregation and specific therapy.[29,30]

Covalent organic frameworks (COFs) have become promising drug delivery carriers due to their unique advantages such as low density, large specific surface area, adjustable pore structure, easy functionalization, and good biocompatibility.[31−34] The inherent adjustable porous channel of COFs is also conducive to the storage of oxygen. COF-based nanocarriers, therefore, also hold tremendous promise in improving the efficiency of PDT therapy.[35−38] In addition, guanidine polymers are cationic antimicrobials that can interact with negatively charged bacteria and have a good bactericidal effect.[39−42] Therefore, the combination of guanidinium-based COFs with intelligent phototherapy agents is expected to achieve precise and efficient synergetic therapy.

https://doi.org/10.1021/acsami.1c05705
ACS Appl. Mater. Interfaces 2021, 13, 27895−27903

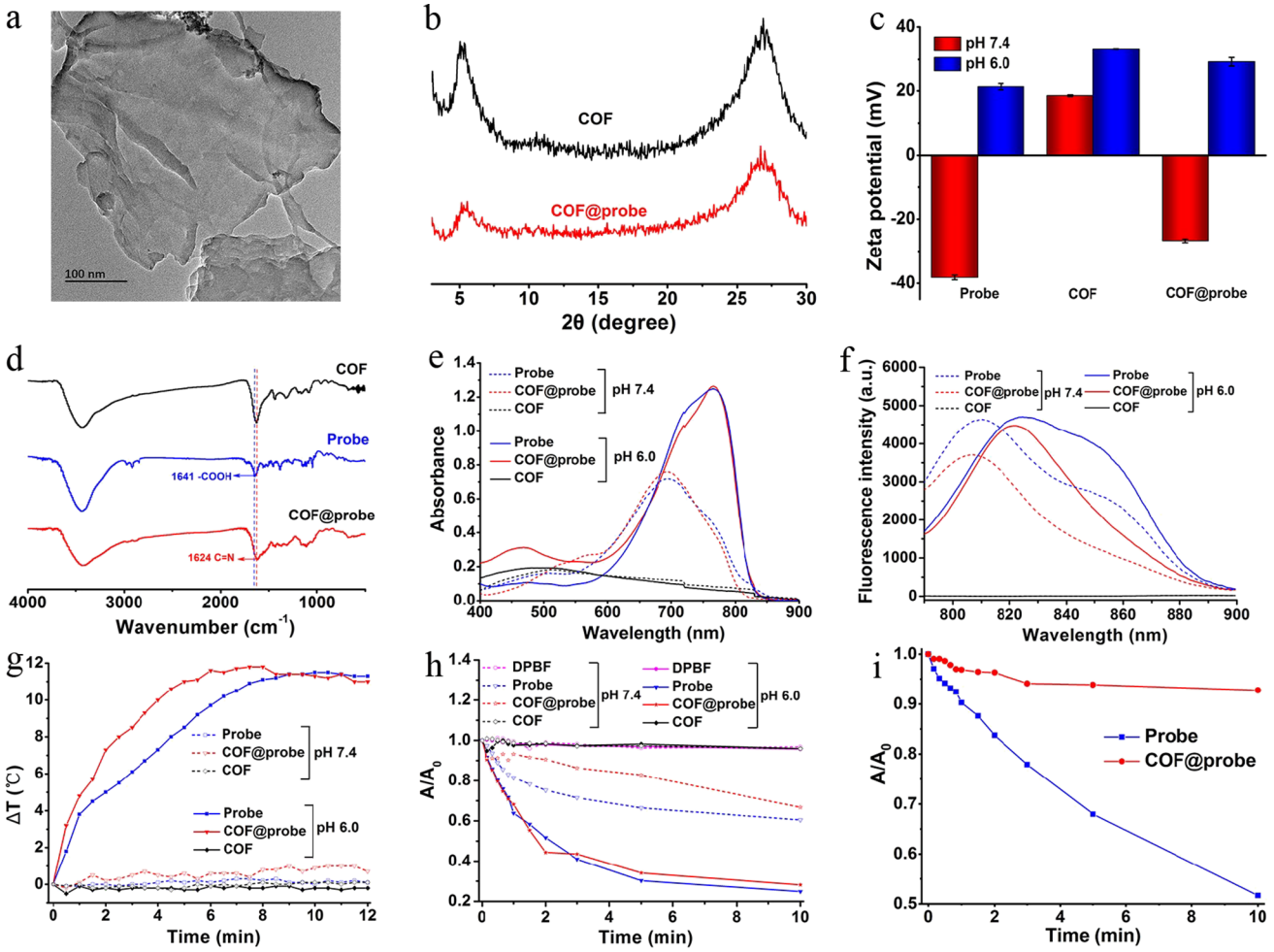

Figure 2. Characterization of COF@probe: (a) Transmission electron microscopy (TEM) image of COF@probe. (b) XRD patterns of the COF and COF@probe. (c) Zeta potentials of the probe, COF, and COF@probe. (d) FT-IR spectra of the probe, COF, and COF@probe. (e) UV−vis−NIR absorption spectra of the probe (1×10^{-5} mol L^{-1}), COF (0.25 mg mL^{-1}), and COF@probe (0.25 mg mL^{-1}, 1×10^{-5} mol L^{-1} as the probe) at pH 7.4 and pH 6.0. (f) Fluorescence spectra of the probe, COF, and COF@probe at pH 7.4 and pH 6.0. (g) Temperature curves of the probe (2×10^{-5} mol L^{-1}), COF (0.5 mg mL^{-1}), and COF@probe (0.5 mg mL^{-1}) with irradiation time under 0.6 W cm^{-2} of 808 nm laser irradiation at pH 7.4 and pH 6.0. (h) Time-dependent absorbance of DPBF at 417 nm (A/A_0) irradiated with an 808 nm laser with and without the probe or COF@probe at pH 6.0 and 7.4. A_0 and A are the initial absorbance of DPBF and the absorbance under definite irradiation time, respectively. (i) Time-dependent absorbance of the probe and COF@probe at pH 7.4 within 10 min of 808 nm laser irradiation (0.6 W cm^{-2}). A_0 is the initial absorbance of the probe or COF@probe, while A is the absorbance of the probe or COF@probe at a certain irradiation time.

Herein, we report a rational strategy for design and fabrication of a pH-reverse switchable chemo/PTT/PDT synergistic therapy nanoplatform based on a PTT/PDT-in-one near-infrared (NIR) agent integrated with an ionic guanidinium-based COF for intelligent bacterial-targeting imaging-guided precision therapy. A pH-responsive hydroxyethyl piperazine-functionalized cyanine is prepared as both fluorescence imaging (FLI) unit and PTT/PDT-in-one therapeutic agent (probe). Meanwhile, the ionic guanidinium-based COF is designed as a nanocarrier and quenching unit to further fabricate the theranostic platform via electrostatic self-assembly to prolong blood circulation, provide charge-reversed smart target ability, and improve the therapeutic effect. The as-prepared COF@probe theranostic platform exhibits smart bacterial-targeted imaging with little background and tissue autofluorescence interference and shows strong chemo/PTT/PDT synergistic bactericidal effect with little side effect, holding great potential for practical application.

RESULTS AND DISCUSSION

Design, Preparation, and Characterization of COF@probe. The design and fabrication of the COF@probe theranostic platform for NIR FLI-guided precision chemo/PTT/PDT synergistic sterilization is illustrated in Figure 1. We design and synthesize a hydroxyethyl piperazine-functionalized cyanine dye as the FLI/PTT/PDT-in-one agent for smart bacterial-targeting FLI and PTT/PDT synergistic sterilization (Figures 1a and S1−S4). The *N* atoms on the piperazine ring serve as the specific recognition site of a bacterial acidic microenvironment to realize smart charge-reversed targeting and specific sterilization. The carboxyl group is introduced into the PTT/PDT-in-one agent to increase hydrophilicity and provide self-assembly sites. Meanwhile, the COF is prepared as an auxiliary bactericidal agent, nanocarrier, and quenching unit via the condensation reaction of aminoguanidine (TG_{Cl}) and 2,5-dihydroxy-1,4-benzenedicarboxaldehyde (Dha) in a teflon-lined stainless steel autoclave (Figure 1b). A COF@probe theranostic platform is subsequently fabricated via electrostatic

https://doi.org/10.1021/acsami.1c05705
ACS Appl. Mater. Interfaces 2021, 13, 27895−27903

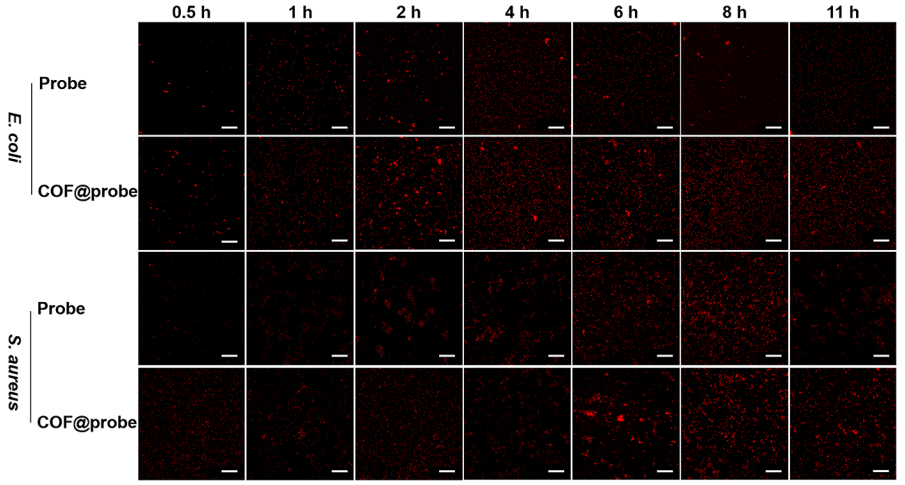

Figure 3. CLSM images of *E. coli* and *S. aureus* treated with the probe or COF@probe. Scale bar, 30 μm.

self-assembly of the above probe and COF to provide charge reversal smart target ability, prolong blood circulation, and improve the therapeutic effect (Figure 1c,d). As such, the designed COF@probe theranostic platform enables precision bactericidal-targeting imaging-guided chemo/PTT/PDT synergistic sterilization.

The prepared COF@probe was exhibited a nanosheet structure with two characteristic diffraction peaks at 5.2 and 27.3° (Figure 2a,b), similar to the initial COF (Figure S5c). Self-assembly of the COF and probe at pH 7.4 (simulated normal physiological pH) turned the zeta potential from 18.5 ± 0.2 to −26.7 ± 0.4 mV as the positive charge of the guanidine group in the COF is neutralized with the negative charge of the carboxyl group in the probe, while change of pH from 7.4 to 6.0 (simulated bacterial acidic microenvironment) made the zeta potential quickly reverse to 29.3 ± 0.3 mV (Figure 2c) because of the protonation and desorption of the probe from the COF. The above results confirm that the as-prepared COF@probe possesses pH-mediated charge-conversion feature, ensuring the long blood circulation and smart bacterial-targeting accumulation. The characteristic stretching vibration peaks appeared in the Fourier transform infrared (FT-IR) spectra at 1624 cm^{-1} (−C═N− of the COF) and 1641 cm^{-1} (−COOH of the probe) verified the successful preparation of COF@probe (Figures 2d and S5a,b). In addition, the color change of COF@probe from brown of the original COF to dark green also confirmed the successful assembly.

The prepared COF@probe gave a characteristic NIR absorption peak at ca. 690 nm at pH 7.4 but showed an obvious red-shifted peak at 770 nm when the pH was adjusted to 6.0 (Figure 2e) and vice versa. Meanwhile, the intensity and position of the two characteristic absorption peaks were not significantly different from those of the probe with the same concentration, indicating that the self-assembly of the COF and probe did not change the intrinsic absorption property of the probe (Figures 2e and S6). However, self-assembly of the COF with the probe at pH 7.4 led to obvious fluorescence quenching of the probe due to the intramolecular and intermolecular fluorescence quenching originating from the aggregation of the probe and the $\pi-\pi$ stacking between the probe and COF, resulting in a low-background signal nanoplatform, while almost all the adsorbed probe was desorbed from the COF and well dispersed in the solvent in the acidic environment, resulting in an activated fluorescence with a characteristic NIR emission peak at 825 nm due to the protonation of *N* atoms in the hydroxyethyl piperazine ring accompanied with charge reversal and inhibiting the photo-induced electron transfer process (Figures 2f and S7a). The pKa and the pH sensitive range of the probe measured by fluorescence titration were 6.3 and 5.5−7.5, respectively (Figures S6 and S7), which were consistent with the bacterial acidic microenvironment.[36] In addition, the prepared COF@probe hold excellent stability at pH 7.4 due to the negligible change in the absorption spectra (Figure S8a,b). The above results confirm that the prepared COF@probe hold great potential for bacterial-specific imaging and imaging-guided PTT/PDT sterilization. The concentration of the probe adsorbed onto the surface of COF@probe (0.5 mg mL^{-1} as the COF) was determined to be 2×10^{-5} mol L^{-1} via UV−vis−NIR absorption spectrometry (Figure S8c,d).

PTT and PDT Performance of COF@probe. The PTT property of the probe under 808 nm laser irradiation with different powers was first explored. The temperature of the probe solution increased significantly and displayed power density and concentration-dependent hyperthermia at pH 6.0 (Figures 2g and S9). In contrast, both phosphate buffer (PBS) and the highest test concentration of the probe at pH 7.4 did not give any increase in temperature during the whole irradiation process (10 min, 0.6 W cm^{-2}) (Figures 2g and S9). The PDT efficiency was then evaluated with 1,3-diphenylisobenzofuran (DPBF) as the singlet oxygen ($^1O_2$) indicator. The decrease in the absorbance of DPBF at 417 nm was used as the basis for judgment.[13] Probe generated significant $^1O_2$ at pH 6.0 upon 808 nm laser irradiation for 10 min (0.6 W cm^{-2}), which was confirmed by the rapid decline in the absorbance of DPBF. However, the probe at pH 7.4 only presented a weak ability to produce $^1O_2$ with slightly decreased absorbance of DPBF (Figures 2h and S10). These results clearly indicate that the probe has great potential for intelligent bacterial-specific phototherapy.

Acid-activated PTT and PDT properties of COF@probe were then investigated under exposure (808 nm laser, 0.6 W cm^{-2}). COF@probe at pH 6.0 exhibited a significant increase of temperature within 10 min 808 nm laser irradiation and displayed a faster heating rate than the probe with the same concentration (Figures 2g and S9b), due to the enhanced photostability of the probe by self-assembly (Figure 2i). In

https://doi.org/10.1021/acsami.1c05705
ACS Appl. Mater. Interfaces 2021, 13, 27895−27903

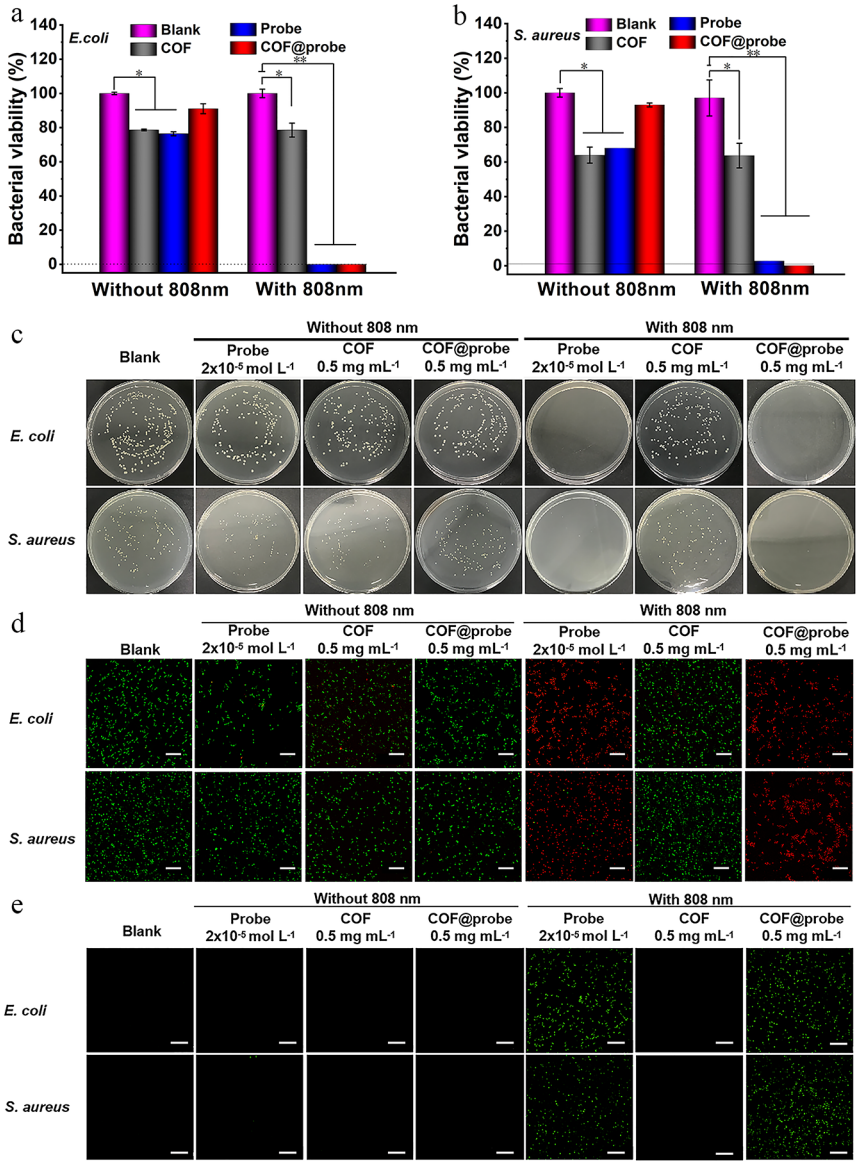

Figure 4. Dark toxicity and chemo/PTT/PDT synergetic antimicrobial effect: (a) and (b) Dark toxicity and chemo/PTT/PDT synergetic antimicrobial effect of the COF (0.5 mg mL^{-1}), probe (2×10^{-5} mol L^{-1}), and COF@probe (0.5 mg mL^{-1}, 2×10^{-5} mol L^{-1} as the probe) to (a) *E. coli* and (b) *S. aureus* (statistical significance: *, $P < 0.05$ and **, $p < 0.01$). (c) Flat colony photographs of bacterial colonies after different treatments. (d) CLSM imaging of bacteria incubated with or without the probe, COF, or COF@probe exposed to an 808 nm laser (0.6 W cm^{-2}, 10 min). Live and dead bacteria were stained with Calcein-AM or PI in green and red, respectively. (e) CLSM images of bacterial colonies after different treatments for the detection of $^1O_2$. Scale bar, 30 μm.

comparison, neither the COF nor COF@probe trigger any obvious temperature increase at pH 7.4 (Figure 2g). Moreover, COF@probe had a strong $^1O_2$ production ability at pH 6.0 with a similar generation efficiency of the probe as proved by the obviously decreased absorbance of DPBF (Figures 2h and S10). However, COF@probe weakened the original weak $^1O_2$ production ability of the probe at pH 7.4 due to the aggregation quenching, which is conducive to practical applications. The above results fully confirm that the PTT/PDT properties of COF@probe could be activated only in the acidic microenvironment, ensuring precision bacterial-specific sterilization without obvious side effects.

In Vitro Imaging and Antibacterial Properties of COF@probe. The potential bacterial-targeting imaging and chemo/PTT/PDT antibacterial effect of COF@probe were investigated with two common foodborne pathogens, *E. coli* and *S. aureus*. The optimal incubation time and the bacterial-targeting ability of COF@probe were first studied via confocal laser scanning microscopy (CLSM). The fluorescence signal rapidly appeared in *E. coli* co-cultured with COF@probe with the crest value at ca. 2−4 h and kept clear up at least 11 h (Figure 3), while the fluorescence-imaging signal of the probe group reached the maximum at ca. 2 h and then weakened rapidly with metabolism. In addition, the fluorescence intensity of *E. coli* treated with the COF@probe group was always stronger than that of the probe at the corresponding time point. The *S. aureus* experiment group reached a consistent conclusion, except that the maximum endocytosis appeared at ca. 6 h (Figure 3). The above results indicate that COF@probe has excellent bacterial target ability and blood circulation. In addition, 6 h was chosen as the optimal co-incubation time for subsequent studies.

https://doi.org/10.1021/acsami.1c05705
ACS Appl. Mater. Interfaces 2021, 13, 27895−27903

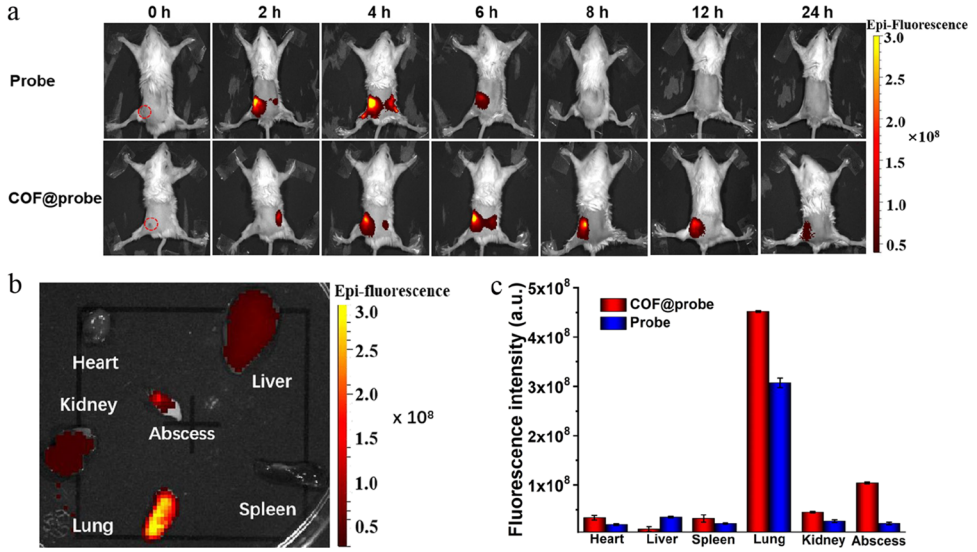

Figure 5. In vivo imaging of COF@probe: (a) Time-dependent NIR fluorescence images of *S. aureus* infection-bearing mice after intravenous injection with the probe or COF@probe. (b) Ex vivo FLI of main organs and abscesses dissected from the mice after injection with COF@probe for 6 h. (c) Fluorescence intensity of abscess and main organs in the mice at 6 h after injection with the probe and COF@probe.

The dark toxicity and chemo/PTT/PDT effect of COF@probe were then investigated through the flat colony counting and live/dead bacterial staining method with calcein acetoxymethyl ester and propidium iodide (Calcein-AM/PI). The bacterial viability of *E. coli* and *S. aureus* treated with COF@probe remained more than 90% even with the test dose of up to 0.5 mg mL^{-1} (Figure 4a,b), which is slightly higher than that of the probe group (Figures 4a,b and S11a) but obviously superior to that of the COF group (70% of *S. aureus* and 80% of *E. coli*) at the same concentration (Figures 4a,b and S11b). This phenomenon is ascribed to the positive charge of the guanidine group in the COF, which can combine with the carboxylate and phosphate on the surface of the bacterial membrane, breaking the charge balance of the membrane and causing the membrane rupture. In contrast, COF@probe showed an excellent bactericidal effect under 808 nm laser irradiation at the acidic microenvironment of bacteria, which is significantly stronger than the same concentration of the COF and slightly better than the same concentration of the probe (Figure 4a–c). The same conclusion was obtained by Calcein-AM/PI staining (Figure 4d). All the above results clearly show that COF@probe not only enhances the biocompatibility but also achieves efficient and rapid sterilization at the acidic environment of bacteria.

To further verify the sterilization effect of COF@probe by PTT/PDT synergistic effect, the variation in temperature and the generation of $^1O_2$ were monitored by NIR thermal imaging and CLSM imaging with 2′,7′-dichlorodihydrofluorescein diacetate (DCFH-DA) as an $^1O_2$ indicator.[43] The bacterial suspension co-incubated with COF@probe showed a strong temperature fluctuation (ca. 8 °C) and a significant fluorescence signal after 10 min 808 nm laser exposure, whereas other control groups had no obvious temperature variation and fluorescence signal (Figure 4e and Figure S12), indicating that the sterilization effect of COF@probe is indeed related to the increase in temperature and the production of $^1O_2$.

In Vivo Bacterial-Targeting Imaging and Precision Chemo/PTT/PDT Synergetic Sterilization. In vitro bacterial-targeting imaging and high antibacterial efficiency of COF@probe encouraged us to assess whether it was qualified to in vivo precision imaging-guided chemo/PTT/PDT sterilization. For this purpose, the biocompatibility of COF@probe was primarily investigated by the MTT assay with 3T3 cells as model cells. The cell viability of 3T3 treated with COF@probe retained more than 95% after 24 h co-culture even at a test concentration of 0.5 mg mL^{-1} (Figure S13), slightly higher than that incubated with the same concentration of the probe (ca. 92%) and COF (ca. 84%), proving that the prepared COF@probe had good biocompatibility, which was improved by the electrostatic self-assembly strategy.

In vivo imaging performance was then explored via intravenous injection with COF@probe or the probe into the *S. aureus*-infected mice. The fluorescence signal in the infection site of the COF@probe treatment group was lightened up at about 4 h and gradually increased to the crest value at ca. 6 h. Meanwhile, the fluorescence signal kept clear up to ca. 24 h, obviously superior to that of the probe group (Figure 5a), indicating that COF@probe holds great promise in in vivo bacterial-targeting imaging and the self-assembled COF@probe does help to prolong blood circulation. In addition, 6 h post-injection with the maximum accumulated amount was determined as the most suitable time point for subsequent treatment. Main organs and abscesses were dissected and collected at 6 h after intravenous injection for ex vivo FLI to more intuitively observe the targeted accumulation and distribution of COF@probe. The fluorescence signals were unavoidable in the reticuloendothelial system organs (such as the lung, liver, and kidney), but only obvious fluorescence signal existed in abscess of the mice injected with COF@probe, which further shows that COF@probe is capable of precision bacterial infection-targeting imaging (Figures 5b,c and S14).

In vivo chemo/PTT/PDT synergetic therapy effect of COF@probe was then studied. For this purpose, *S. aureus* infection-bearing mice were established and divided into four groups randomly. The experimental group refers to the mice intravenously injected with COF@probe and subjected to 808 nm laser exposure. Other three control groups include the mice without treatment, the mice injected with PBS with 808

https://doi.org/10.1021/acsami.1c05705
ACS Appl. Mater. Interfaces 2021, 13, 27895−27903

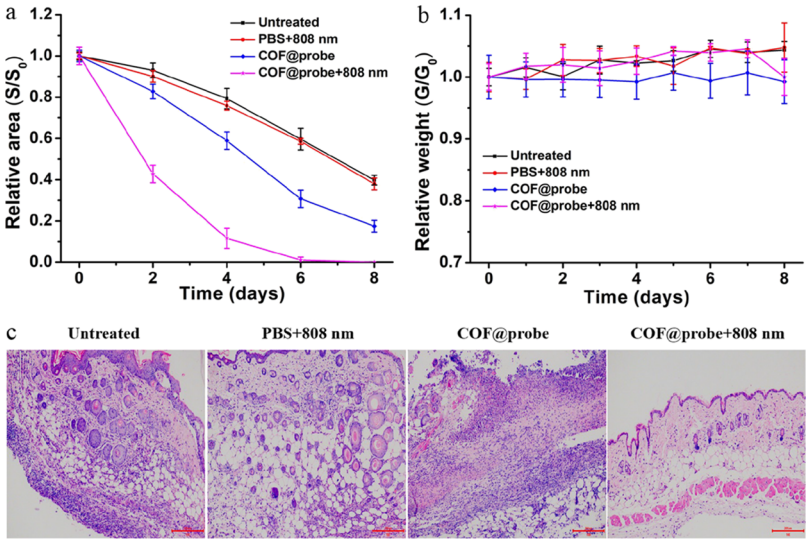

Figure 6. COF@probe-mediated in vivo chemo/PTT/PDT synergetic therapy effect in the *S. aureus* infection-bearing mice model: (a) Time-dependent relative area of the infected wound of mice under various treatments. S_0 and S are the areas of infected wound before treatment and at a certain therapy point, respectively. (b) Time-dependent relative body weight of mice under various treatments. G_0 is the initial weight of mice of different groups, while G is the weight at a certain therapy point. (c) H&E staining of abscesses of mice after different treatments for 8 days. Scale bar, 100 μm.

nm laser irradiation, and the mice treated with COF@probe only. The temperature of abscesses rose rapidly within 10 min irradiation in the treatment group, while the temperature of the control group hardly changed, indicating that the COF@probe has effective PTT effect and 0.6 W cm^{-2} of 808 nm laser itself is biosafe without heat damage (Figure S15). The abscesses of mice in the experimental group gradually alleviated and healed completely after 8 days; the healing rate was observably faster than that of the control groups (Figures 6a and S16). In addition, the control group treated with COF@probe showed a weak healing effect compared to the other two control groups, indicating that the PTT/PDT effect of COF@probe was specifically regulated by the bacterial acidic microenvironment and COF@probe itself has a certain antibacterial effect.

Hematoxylin and eosin (H&E) staining of the abscesses and organs was performed after 8 days. A large number of necrotic cells and neutrophils were present in the infected site of the control mice, whereas the skin of the experimental group produced new blood vessels and fibroblasts (Figure 6c), demonstrating the highly effective antibacterial activity of COF@probe against *S. aureus* under 808 nm laser irradiation. In addition, significant reduction of the blood neutrophilic granulocyte percentage in the COF@probe group was also confirmed by the blood cell analysis (Figure S17). Moreover, no obvious organ necrosis and inflammation and body weight change was observed in both experimental and control groups, showing that COF@probe had no obvious side effects (Figures 6b and S18). The above results consistently confirm that the developed COF@probe is qualified to precision bacterial-targeting guided excellent sterilization without obvious side effects.

CONCLUSIONS

In conclusion, we have reported a COF@probe platform for precision FLI-guided chemo/PTT/PDT synergistic sterilization. The COF@probe nanoplatform combines the merits of good biocompatibility, enhanced blood circulation, charge reversal smart targeting capability, pH reversibly activated NIR FLI, and chemo/PTT/PDT synergistic enhanced sterilization, ensuring the precision imaging and excellent sterilization with little damage to normal tissues. We believe that the smart self-assembly strategy with integration of the charge reversal targeting and reversibly activated imaging and PTT/PDT-in-one therapeutic effect provides a forward-looking strategy to design more intelligent platforms for bacterial infections.

ASSOCIATED CONTENT

Supporting Information

The Supporting Information is available free of charge at https://pubs.acs.org/doi/10.1021/acsami.1c05705.

Additional information including chemicals and materials, instrumentation, synthetic procedures, experimental details, and supplementary figures as mentioned in the text (PDF)

AUTHOR INFORMATION

Corresponding Authors

Xu Zhao − *State Key Laboratory of Food Science and Technology, International Joint Laboratory on Food Safety, and Institute of Analytical Food Safety, School of Food Science and Technology, Jiangnan University, Wuxi 214122, China;* orcid.org/0000-0001-8000-9045; Email: zhaoxu2017@jiangnan.edu.cn

Xiu-Ping Yan − *State Key Laboratory of Food Science and Technology, International Joint Laboratory on Food Safety, Institute of Analytical Food Safety, School of Food Science and Technology, and Key Laboratory of Synthetic and Biological Colloids, Ministry of Education, School of Chemical and Material Engineering, Jiangnan University, Wuxi 214122, China;* orcid.org/0000-0001-9953-7681; Email: xpyan@jiangnan.edu.cn

Authors

Yu-Shi Liu − *Institute of Analytical Food Safety, School of Food Science and Technology, Jiangnan University, Wuxi 214122, China*

Xiang Wei − *Institute of Analytical Food Safety, School of Food Science and Technology, Jiangnan University, Wuxi 214122, China*

Li-Jian Chen − *State Key Laboratory of Food Science and Technology, International Joint Laboratory on Food Safety, and Institute of Analytical Food Safety, School of Food Science and Technology, Jiangnan University, Wuxi 214122, China;* orcid.org/0000-0001-8671-8766

Complete contact information is available at: https://pubs.acs.org/10.1021/acsami.1c05705

Notes

The authors declare no competing financial interest.

■ ACKNOWLEDGMENTS

The authors appreciate the support from the National Natural Science Foundation of China (No. 21934002, 21804056, and 21804057), the Natural Science Foundation of Jiangsu Province, China (No. BK20180581 and BK20180584), the China Postdoctoral Science Foundation (No. 2018 M630511), and Collaborative Innovation Center of Food Safety and Quality Control in Jiangsu Province.

■ REFERENCES

(1) Hou, X. X.; Yang, L. J.; Liu, J. J.; Zhang, Y. M.; Chu, L. P.; Ren, C. Y.; Huang, F.; Liu, J. F. Silver-Decorated, Light-Activatable Polymeric Antimicrobials for Combined Chemo-Photodynamic Therapy of Drug-Resistant Bacterial Infection. *Biomater. Sci.* **2020**, *8*, 6350−6361.

(2) Jia, Q. Y.; Song, Q.; Li, P.; Huang, W. Rejuvenated Photodynamic Therapy for Bacterial Infections. *Adv. Healthc. Mater.* **2019**, *8*, No. 1900608.

(3) Jiang, Q.; E, F.; Tian, J.; Yang, J.; Zhang, J.; Cheng, Y. Light-Excited Antibiotics for Potentiating Bacterial Killing via Reactive Oxygen Species Generation. *ACS Appl. Mater. Interfaces* **2020**, *12*, 16150−16158.

(4) Qiu, H. Y.; Zhu, S. Q.; Pang, L. L.; Ma, J. Q.; Liu, Y. J.; Du, L. N.; Wu, Y.; Jin, Y. G. ICG-Loaded Photodynamic Chitosan/Polyvinyl Alcohol Composite Nanofibers: Anti-Resistant Bacterial Affect and Improved Healing of Infected Wounds. *Int. J. Pharm.* **2020**, *588*, No. 119797.

(5) Dai, X. M.; Zhao, Y.; Yu, Y. Y.; Chen, X. L.; Wei, X. S.; Zhang, X. G.; Li, C. X. Single Continuous Near-Infrared Laser-Triggered Photodynamic and Photothermal Ablation of Antibiotic-Resistant Bacteria Using Effective Targeted Copper Sulfide Nanoclusters. *ACS Appl. Mater. Interfaces* **2017**, *9*, 30470−30479.

(6) Yuan, Z.; Lin, C. C.; He, Y.; Tao, B. L.; Chen, M. W.; Zhang, J. X.; Liu, P.; Cai, K. Y. Near-Infrared Light-Triggered Nitric-Oxide Enhanced Photodynamic Therapy and Low Temperature Photothermal Therapy for Biofilm Elimination. *ACS Nano* **2020**, *14*, 3546−3562.

(7) Lu, C. B.; Sun, F. F.; Liu, Y. Y.; Xiao, Y.; Qiu, Y. H.; Mu, H. B.; Duan, J. Y. Versatile Chlorin e6-Based Magnetic Polydopamine Nanoparticles for Effectively Capturing and Killing MRSA. *Carbohydr. Polym.* **2019**, *218*, 289−298.

(8) Bilici, K.; Atac, N.; Muti, A.; Baylam, I.; Dogan, O.; Sennaroglu, A.; Can, F.; Yagci Acar, H. Broad Spectrum Antibacterial Photodynamic and Photothermal Therapy Achieved with Indocyanine Green Loaded SPIONs under Near Infrared Irradiation. *Biomater. Sci.* **2020**, *8*, 4616−4625.

(9) Wang, D.; Niu, L. J.; Qiao, Z. Y.; Cheng, D. B.; Wang, J. F.; Zhong, Y.; Bai, F.; Wang, H.; Fan, H. Y. Synthesis of Self-Assembled Porphyrin Nanoparticle Photosensitizers. *ACS Nano* **2018**, *12*, 3796−3803.

(10) Sun, J.; Song, L. J.; Fan, Y.; Tian, L. M.; Luan, S. F.; Niu, S. C.; Ren, L. Q.; Ming, W. H.; Zhao, J. Synergistic Photodynamic and Photothermal Antibacterial Nanocomposite Membrane Triggered by Single NIR Light Source. *ACS Appl. Mater. Interfaces* **2019**, *11*, 26581−26589.

(11) Zhou, K.; Qiu, X. Y.; Xu, L. T.; Li, G. P.; Rao, B.; Guo, B. L.; Pei, D. D.; Li, A.; He, G. Poly(selenoviologen)-Assembled Upconversion Nanoparticles for Low-Power Single-NIR Light-Triggered Synergistic Photodynamic and Photothermal Antibacterial Therapy. *ACS Appl. Mater. Interfaces* **2020**, *12*, 26432−26443.

(12) Wang, D. W.; Zhang, Z.; Lin, L.; Liu, F.; Wang, Y. B.; Guo, Z. P.; Li, Y. H.; Tian, H. Y.; Chen, X. S. Porphyrin-Based Covalent Organic Framework Nanoparticles for Photoacoustic Imaging-Guided Photodynamic and Photothermal Combination Cancer Therapy. *Biomaterials* **2019**, *223*, No. 119459.

(13) Zhang, Y. X.; Huang, P.; Wang, D.; Chen, J. C.; Liu, W. Z.; Hu, P.; Huang, M. D.; Chen, X. Y.; Chen, Z. Near-Infrared-Triggered Antibacterial and Antifungal Photodynamic Therapy Based on Lanthanide-Doped Upconversion Nanoparticles. *Nanoscale* **2018**, *10*, 15485−15495.

(14) Li, M.; Liu, X. M.; Tan, L.; Cui, Z. D.; Yang, X. J.; Li, Z. Y.; Zheng, Y. F.; Yeung, K. W. K.; Chu, P. K.; Wu, S. L. Noninvasive Rapid Bacteria-Killing and Acceleration of Wound Healing through Photothermal/Photodynamic/Copper Ion Synergistic Action of a Hybrid Hydrogel. *Biomater. Sci.* **2018**, *6*, 2110−2121.

(15) Liu, W. Z.; Zhang, Y. X.; You, W. W.; Su, J. Q.; Yu, S. H.; Dai, T.; Huang, Y. M.; Chen, X. Y.; Song, X. R.; Chen, Z. Near-Infrared-Excited Upconversion Photodynamic Therapy of Extensively Drug-Resistant Acinetobacter Baumannii Based on Lanthanide Nanoparticles. *Nanoscale* **2020**, *12*, 13948−13957.

(16) Li, X. S.; Kolemen, S.; Yoon, J.; Akkaya, E. U. Activatable Photosensitizers: Agents for Selective Photodynamic Therapy. *Adv. Funct. Mater.* **2017**, *27*, No. 1604053.

(17) Li, X. S.; Lee, D. Y.; Huang, J. D.; Yoon, J. Phthalocyanine-Assembled Nanodots as Photosensitizers for Highly Efficient Type I Photoreactions in Photodynamic Therapy. *Angew. Chem. Int. Ed.* **2018**, *57*, 9885−9890.

(18) Cui, W.; Li, J. B.; Decher, G. Self-Assembled Smart Nanocarriers for Targeted Drug Delivery. *Adv. Mater.* **2016**, *28*, 1302−1311.

(19) Colilla, M.; Vallet-Regí, M. Targeted Stimuli-Responsive Mesoporous Silica Nanoparticles for Bacterial Infection Treatment. *Int. J. Mol. Sci.* **2020**, *21*, No. 8605.

(20) Zhao, Z. W.; Yan, R.; Wang, J. H.; Wu, H.; Wang, Y. H.; Chen, A. H.; Shao, S. L.; Li, Y. Q. A Bacteria-Activated Photodynamic Nanosystem Based on Polyelectrolyte-Coated Silica Nanoparticles. *J. Mater. Chem. B* **2017**, *5*, 3572−3579.

(21) Niu, N.; Zhou, H. P.; Liu, N.; Jiang, H.; Hua, Z. Z.; Yu, C. A Perylene-Based Membrane Intercalating Conjugated Oligoelectrolyte with Efficient Photodynamic Antimicrobial Activity. *Chem. Commun.* **2019**, *55*, 4395−4398.

(22) Wu, L. J.; Wu, M.; Lin, X. Y.; Zhang, X. L.; Liu, X. L.; Liu, J. F. Magnetite Nanocluster and Paclitaxel-Loaded Charge-Switchable Nanohybrids for MR Imaging and Chemotherapy. *J. Mater. Chem. B* **2017**, *5*, 849−857.

(23) Nederberg, F.; Zhang, Y.; Tan, J. P. K.; Xu, K. J.; Wang, H. Y.; Yang, C.; Gao, S. J.; Guo, X. D.; Fukushima, K.; Li, L. J.; Hedrick, J. L.; Yang, Y. Y. Biodegradable Nanostructures with Selective Lysis of Microbial Membranes. *Nat. Chem.* **2011**, *3*, 409−414.

(24) Wang, Y. Q.; Jin, Y. Y.; Chen, W.; Wang, J. J.; Chen, H.; Sun, L.; Li, X.; Ji, J.; Yu, Q.; Shen, L. Y.; Wang, B. L. Construction of Nanomaterials with Targeting Phototherapy Properties to Inhibit Resistant Bacteria and Biofilm Infections. *Chem. Eng. J.* **2019**, *358*, 74−90.

(25) Radovic-Moreno, A. F.; Lu, T. K.; Puscasu, V. A.; Yoon, C. J.; Langer, R.; Farokhzad, O. C. Surface Charge-Switching Polymeric Nanoparticles for Bacterial Cell Wall-Targeted Delivery of Antibiotics. *ACS Nano* **2012**, *6*, 4279−4287.

(26) Park, W.; Park, S.; Shin, H.; Na, K. Acidic Tumor pH-Responsive Nanophotomedicine for Targeted Photodynamic Cancer Therapy. *J. Nanomater.* **2016**, *2016*, 1−8.

(27) Zhao, X.; Zhao, K. C.; Chen, L. J.; Liu, Y. S.; Liu, J. L.; Yan, X. P. pH Reversibly Switchable Nanocapsule for Bacteria-Targeting Near Infrared Fluorescence Imaging-Guided Precision Photodynamic Sterilization. *ACS Appl. Mater. Interfaces* **2020**, *12*, 45850−45858.
(28) Wang, C. L.; Chen, P.; Qiao, Y. B.; Kang, Y.; Yan, C. R.; Yu, Z.; Wang, J.; He, X.; Wu, H. pH Responsive Superporogen Combined with PDT Based on Poly Ce6 Ionic Liquid Grafted on SiO_2 for Combating MRSA Biofilm Infection. *Theranostics* **2020**, *10*, 4795−4808.
(29) Chen, H.; Jin, Y. Y.; Wang, J. J.; Wang, Y. Q.; Jiang, W. Y.; Dai, H. D.; Pang, S. Y.; Lei, L.; Ji, J.; Wang, B. L. Design of Smart Targeted and Responsive Drug Delivery Systems with Enhanced Antibacterial Properties. *Nanoscale* **2018**, *10*, 20946−20962.
(30) Li, S.; Zhao, Z. X.; Wu, W.; Ding, C. M.; Li, J. S. Dual pH-Responsive Micelles with Both Charge-Conversional Property and Hydrophobic-Hydrophilic Transition for Effective Cellular Uptake and Intracellular Drug Release. *Polym. Chem.* **2016**, *7*, 2202−2208.
(31) Liu, S. N.; Zhou, Y.; Hu, C. L.; Cai, L. H.; Pang, M. L. Covalent Organic Framework-Based Nanocomposite for Synergetic Photo-, Chemodynamic-, and Immunotherapies. *ACS Appl. Mater. Interfaces* **2020**, *12*, 43456−43465.
(32) Guan, Q.; Wang, G. B.; Zhou, L. L.; Li, W. Y.; Dong, Y. B. Nanoscale Covalent Organic Frameworks as Theranostic Platforms for Oncotherapy: Synthesis, Functionalization, and Applications. *Nanoscale Adv.* **2020**, *2*, 3656−3733.
(33) Feng, L. L.; Qian, C.; Zhao, Y. L. Recent Advances in Covalent Organic Framework-Based Nanosystems for Bioimaging and Therapeutic Applications. *ACS Materials Lett.* **2020**, *2*, 1074−1092.
(34) Tong, X. N.; Gan, S. J.; Wu, J. H.; Hu, Y. Q.; Yuan, A. H. A Nano-Photosensitizer Based on Covalent Organic Framework Nanosheets with High Loading and Therapeutic Efficacy. *Nanoscale* **2020**, *12*, 7376−7382.
(35) Wang, K.; Zhang, Z.; Lin, L.; Chen, J.; Hao, K.; Tian, H. Y.; Chen, X. S. Covalent Organic Nanosheets Integrated Heterojunction with Two Strategies to Overcome Hypoxic-Tumor Photodynamic Therapy. *Chem. Mater.* **2019**, *31*, 3313−3323.
(36) Zhu, W. W.; Liu, J. J.; Dong, Z. L.; Liu, Z. pH-Responsive Nanoscale Covalent Organic Polymers as a Biodegradable Drug Carrier for Combined Photodynamic Chemotherapy of Cancer. *ACS Appl. Mater. Interfaces* **2018**, *10*, 14475−14482.
(37) Guan, Q.; Zhou, L. L.; Li, W. Y.; Li, Y. A.; Dong, Y. B. Covalent Organic Frameworks (COFs) for Cancer Therapeutics. *Chem. A Eur. J.* **2020**, *26*, 5583−5591.
(38) Fang, Q. R.; Wang, J. H.; Gu, S.; Kaspar, R. B.; Zhuang, Z. B.; Zheng, J.; Guo, H. X.; Qiu, S. L.; Yan, Y. S. 3D Porous Crystalline Polyimide Covalent Organic Frameworks for Drug Delivery. *J. Am. Chem. Soc.* **2015**, *137*, 8352−8355.
(39) Peng, K. M.; Zou, T.; Ding, W.; Wang, R. N.; Guo, J. S.; Round, J. J.; Tu, W. P.; Liu, C.; Hu, J. Q. Development of Contact-Killing Non-Leaching Antimicrobial Guanidyl-Functionalized Polymers via Click Chemistry. *RSC Adv.* **2017**, *7*, 24903−24913.
(40) Mitra, S.; Kandambeth, S.; Biswal, B. P.; Khayum, M. A.; Choudhury, C. K.; Mehta, M.; Kaur, G.; Banerjee, S.; Prabhune, A.; Verma, S.; Roy, S.; Kharul, U. K.; Banerjee, R. Self-Exfoliated Guanidinium-Based Ionic Covalent Organic Nanosheets (iCONs). *J. Am. Chem. Soc.* **2016**, *138*, 2823−2828.
(41) Da, H. J.; Yang, C. X.; Yan, X. P. Cationic Covalent Organic Nanosheets for Rapid and Selective Capture of Perrhenate: An Analogue of Radioactive Pertechnetate from Aqueous Solution. *Environ. Sci. Technol.* **2019**, *53*, 5212−5220.
(42) Zhang, J. L.; Zhou, M.; Xu, Z. H.; Jiang, C. Y.; Shen, C.; Meng, Q. Guanidyl-Functionalized Graphene/Polysulfone Mixed Matrix Ultrafiltration Membrane with Superior Permselective, Antifouling and Antibacterial Properties for Water Treatment. *J. Colloid Interface Sci.* **2019**, *540*, 295−305.
(43) Zhao, X.; Zhao, K. C.; Chen, L. J.; Liu, Y. S.; Liu, J. L.; Yan, X. P. A pH Reversibly Activatable NIR Photothermal/Photodynamic-in-one Agent Integrated with Renewable Nanoimplants for Image-Guided Precision Phototherapy. *Chem. Sci.* **2021**, *12*, 442−452.

https://doi.org/10.1021/acsami.1c05705
ACS Appl. Mater. Interfaces 2021, 13, 27895−27903